CHAPTER 375

THE EFFECT OF THE CL-VORTEX FORCE IN 3D WAVE-CURRENT INTERACTION

M.W. Dingemans[1], J.A.Th.M. van Kester[2], A.C. Radder[3] and R.E. Uittenbogaard[2]

Abstract

Experiments in flumes (i.e., Kemp and Simons, 1982, 1983, and Klopman, 1994) have shown that the mean current profile for following waves is more uniformly distributed than the corresponding current-only case, whereas the case of an opposing current leads to a more straight profile. This paper is concerned with proving that inclusion of the so-called Craik-Leibovich (CL) vortex force in the mean-current equation gives, at least for a part, an explanation of this phenomenon.

Introduction

For coastal dynamics applications it is essential to have an accurate prediction of the vertical structure of the mean current. The mean current, however, is strongly influenced by the free surface wave motion. Experiments in flumes (i.e., Kemp and Simons, 1982, 1983, and Klopman, 1994) have shown that the mean-current profile for following waves is more uniformly distributed than the corresponding current-only case, whereas the case of an opposing current leads to a more straight profile (see Figure 1). The purpose of this paper is to give a possible expanation of this behaviour. Hereto we consider the so-called Craik-Leibovich (CL) equation, derived by Craik and Leibovich (1976) in which a vortex force is present. The effect of this vortex force on the underlying flow is studied.

First we consider the CL-equation. As it is essential to have shear in the velocity profile, the used turbulence-closure model is subsequently described. Because the CL-equation is also used to describe the formation of Langmuir circulation cells, some properties of these are succintly described next. For numerical evaluations the treatment of the vertical momentum equation is possible in a number

[1]Senior Researcher, Delft Hydraulics, P.O. Box 152, 8300 AD Emmeloord, The Netherlands
[2]Senior Researcher, Delft Hydraulics, P.O. Box 177, 2600 MH Delft, The Netherlands
[3]Senior Researcher, Rijkswaterstaat-RIKZ, P.O. Box 20907, 2500 EX The Hague, The Netherlands

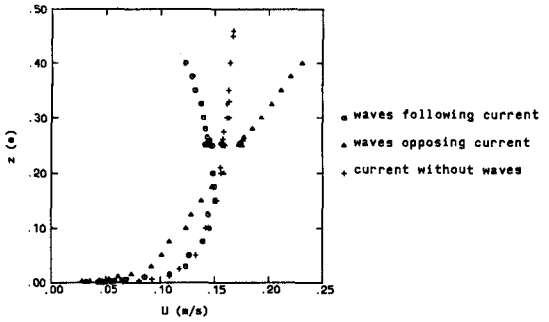

Figure 1: Mean current profiles, after Klopman (1994).

of ways. The most accurate one is described next. Finally the results of some numerical experiments are shown and compared with Klopman's measurements.

The CL equation

When deriving the mean-current equations in so-called Generalised Lagrangian Mean (GLM) coordinates, the following equation is obtained (see Andrews and McIntyre, 1978, Eq. (3.8)):

$$\overline{D}^L\left(\overline{u}_i^L\right) + \frac{1}{\rho_0}\frac{\partial \overline{p}^L}{\partial x_i} - \frac{\overline{\rho}^L}{\rho_0} g_i = \overline{D}^L\left(\overline{P}_i^L\right) + \frac{\partial}{\partial x_i}\left(\frac{1}{2}\left(\overline{u_m^\ell u_m^\ell}\right)\right) + \overline{P}_k^L \frac{\partial \overline{u}_k^L}{\partial x_i}\,, \qquad (1)$$

where $\overline{P}_i^L$ is the pseudo-momentum and $\overline{()}^L$ is the Generalised Lagrangian mean, i.e. the mean over the perturbed position. Summation over repeated indices is used, i.e., the Einstein convention is applied.

Leibovich (1980) has shown that under mild conditions, Eq. (1) reduces to the so-called Craik-Leibovich equation in Eulerian coordinates, which can be written as

$$\frac{\partial \overline{\boldsymbol{u}}}{\partial t} + (\overline{\boldsymbol{u}} \cdot \operatorname{grad})\,\overline{\boldsymbol{u}} + \operatorname{grad}\overline{\pi} = \overline{\boldsymbol{u}}^S \wedge \operatorname{curl}\overline{\boldsymbol{u}}\,, \qquad (2)$$

where the pressure term $\overline{\pi}$ is given by $\overline{\pi} = \dfrac{\overline{p}}{\rho} + gz + \left\langle \dfrac{1}{2}\tilde{\boldsymbol{u}} \cdot \tilde{\boldsymbol{u}} \right\rangle$, $\overline{\boldsymbol{u}}$ is the (Eulerian) mean velocity and $\tilde{\boldsymbol{u}}$ is the wave part of the velocity. The so-called mild conditions for which the approximations are valid, amount to the condition that the waves are primarily dominated by their irrotational part. This implies that either the mean shear or the mean current is relatively weak and we thus have to impose the condition that the current is small with respect to the orbital velocity.

Notice that with $\overline{\boldsymbol{u}}^S = \left(\overline{u}^S, \overline{v}^S, 0\right)^T$ and $\overline{\boldsymbol{u}} = (\overline{u}, \overline{v}, \overline{w})^T$ we have, writing $\overline{\boldsymbol{\omega}} = \operatorname{curl}\overline{\boldsymbol{u}}$,

$\overline{\boldsymbol{T}} = \overline{\boldsymbol{u}}^S \wedge \overline{\boldsymbol{\omega}} =$

$$= \left(\overline{v}^S \left(\frac{\partial \overline{v}}{\partial x} - \frac{\partial \overline{u}}{\partial y} \right), -\overline{u}^S \left(\frac{\partial \overline{v}}{\partial x} - \frac{\partial \overline{u}}{\partial y} \right), \overline{u}^S \left(\frac{\partial \overline{u}}{\partial z} - \frac{\partial \overline{w}}{\partial x} \right) - \overline{v}^S \left(\frac{\partial \overline{w}}{\partial y} - \frac{\partial \overline{v}}{\partial z} \right) \right)^T$$

$$\cong \left(0, \overline{u}^S \frac{\partial \overline{u}}{\partial y}, \overline{u}^S \frac{\partial \overline{u}}{\partial z} \right)^T \equiv \overline{\boldsymbol{T}}_0 \,, \tag{3}$$

where the latter approximations are those of Craik (1982), valid for a flume with x directed along the flume.

Although the inclusion of viscosity is not directly needed, it is needed in an indirect way, otherwise no shear would be present in the mean-current profile. Moreover, once generated vortices should remain bounded in magnitude and this is achieved by taking viscosity into account. Also in view of the application to a wave flume, where the lateral boundary conditions play an important role, we include the viscous stress tensor in the description. Equation (2) then is extended to

$$\frac{\partial \overline{\boldsymbol{u}}}{\partial t} + (\overline{\boldsymbol{u}} \cdot \operatorname{grad}) \overline{\boldsymbol{u}} + \operatorname{grad} \left(gz + \frac{\overline{p}}{\rho} + \left\langle \frac{1}{2} \tilde{\boldsymbol{u}} \cdot \tilde{\boldsymbol{u}} \right\rangle \right) = \overline{\boldsymbol{u}}^S \wedge \overline{\boldsymbol{\omega}} + \frac{1}{\rho} \operatorname{div} \overline{\boldsymbol{\sigma}}' \,, \tag{4}$$

where $\operatorname{div} \overline{\boldsymbol{\sigma}}' \equiv \partial \overline{\sigma}'_{ki} / \partial x_k$ and $\overline{\sigma}'_{ki}$ is given by $\overline{\sigma}'_{ki} = \left(\eta^{(i)} \partial u_k / \partial x_i + \eta^{(k)} \partial u_i / \partial x_k \right)$, while no summation over the indices on η should be performed and the viscosity is usually non-isentropic. However, we take the (eddy) viscosity coefficient to be isentropic because of the scales on which the flow occurs here and the directions. Applying the Boussinesq-hypothesis, the stresses $\overline{\sigma}'_{ki}$ are approximated as

$$\overline{\sigma}'_{ki} = \nu_T \left(\frac{\partial \overline{u}_i}{\partial x_k} + \frac{\partial \overline{u}_k}{\partial x_i} \right) \,, \tag{5}$$

while the eddy viscosity ν_T has still to be determined. In the present case we consider a cross section of the flume, i.e., we take $\partial_{x_1} \equiv 0$.

The turbulence-closure model

For the specification of the eddy-viscosity coefficient ν_T three possibilities were considered.

1. For a constant eddy-viscosity coefficient the velocity profiles near the bottom and the side walls are parabolic. This is physically not correct as for such situations the profiles should be logarithmic; ν_T should be flow-dependent.

2. Prandtl mixing-length model.

   In the Prandtl mixing-length model, the mixing length ℓ is prescribed as a function of the geometry. Because in our case the lateral boundaries are

also of importance, the following variation of Bakhmetev's (1932) choice for shallow-water models is used for the mixing length:

$$\ell = \kappa y\,(b-y)\,(z+h)\left(1-\frac{z+h}{h+\zeta}\right)^{1/2}\,, \tag{6}$$

where b is the width of the flume, h is the still-water depth, ζ is the free-surface elevation and κ is von Karman's costant. This choice for ℓ yields a parabolic profile near the boundaries. As ℓ only depends on the distance to the boundaries, it is independent of the secondary circulations induced by the CL vortex force $\overline{\boldsymbol{T}}_0$. No results from this model are shown.

3. $\mathsf{k}-\epsilon$ model.

In our application of the $\mathsf{k}-\epsilon$ model the advection and dissipation terms in the direction of the flume (the $x-$direction) have been neglected. The transport equations for the kinetic energy k and the dissipation ϵ are then given by

$$\frac{D\mathsf{k}}{Dt} = \nabla\cdot\left[\left(\nu+\frac{\nu_T}{\sigma_k}\right)\nabla\mathsf{k}\right] + P_k - \epsilon \tag{7a}$$

$$\frac{D\epsilon}{Dt} = \nabla\cdot\left[\left(\nu+\frac{\nu_T}{\sigma_\epsilon}\right)\nabla\epsilon\right] + P_\epsilon - \mathrm{c}_{2\epsilon}\frac{\epsilon^2}{\mathsf{k}}\,, \tag{7b}$$

where

$$D/Dt \equiv \partial/\partial t + \boldsymbol{v}\cdot\nabla \quad , \quad \nabla = (0,\partial_y,\partial_z)^T \quad , \quad \boldsymbol{v} = (0,v,w)^T\,, \tag{7c}$$

$$P_k = \frac{1}{2}\nu_T\left|\frac{\partial\overline{u}_k}{\partial x_j}+\frac{\partial\overline{u}_i}{\partial x_k}\right|^2 \quad \text{with} \quad \partial_{x_1}\equiv 0\,, \tag{7d}$$

$$P_\epsilon = \mathrm{c}_{1\epsilon}\frac{\epsilon}{\mathsf{k}}P_k \quad \text{and} \quad \nu_T = \mathrm{c}_\mu\frac{\mathsf{k}^2}{\epsilon} \tag{7e}$$

and the constants are given by the standard setting:

$$\mathrm{c}_\mu = 0.09\,,\ \mathrm{c}_{1\epsilon} = 1.44\,,\ \mathrm{c}_{2\epsilon} = 1.92\,,\ \sigma_k = 1 \text{ and } \sigma_\epsilon = 1.3\,. \tag{7f}$$

Boundary conditions for the $\mathsf{k}-\epsilon$ *model*

The turbulent kinetic energy is imposed both at the side walls and the bed. The pertinent value is obtained by applying local equilibrium between production and dissipation of kinetic energy. This leads to the Dirichlet boundary conditions

$$\mathsf{k}|_{y=0} = \mathsf{k}|_{y=b} = (u_*^s)^2/\sqrt{\mathrm{c}_\mu} \quad \text{and} \quad \mathsf{k}|_{z=-h} = \left(u_*^b\right)^2/\sqrt{\mathrm{c}_\mu} \tag{8a}$$

with u_*^s and u_*^b the shear-stress velocity at the sidewalls and the bottom respectively. The shear-stress velocity u_* is obtained by applying the logarithmic

boundary law for the velocity point nearest to the boundary. With δ half the grid size near the side walls and the bed and z_0 the roughness length, the following relations hold

$$\frac{\overline{u}(\delta)}{u_*} = \frac{1}{\kappa} \log\left(\frac{\delta}{z_0}\right) \quad \text{for a rough wall} \tag{8b}$$

and

$$\frac{\overline{u}(\delta)}{u_*} = \frac{1}{\kappa} \log\left(\frac{\delta u_*}{\nu}\right) + 5.2 \quad \text{for a smooth wall}\,, \tag{8c}$$

where log is the natural logarithm. In the latter case the value u_* is found by iteration. Because a staggered grid is used, the velocity $\overline{u}(\delta)$ is indeed known at the previous time step. At the free surface we take $\mathsf{k} = 0$.

For the transport equation for dissipation rate ϵ we take the following Neumann-type boundary condition:

$$\left.\frac{\partial \epsilon}{\partial z}\right|_{\delta} = -\frac{u_*^3}{\kappa \delta^2}\,, \tag{8d}$$

and at the free surface is taken $\epsilon = 0$.

Langmuir circulations

Equation (4) is basic to the generation of Langmuir circulations by an instability mechanism (Leibovich, 1983). The essential point is that a combination of a 2D shear flow in the vertical xz plane with an irrotational Stokes drift of the wave field in the same direction is unstable to spanwise (i.e., in y) disturbances. Write now the vorticity vector as $\boldsymbol{\omega} = (\omega_x, \omega_y, \omega_z)^T$. Two different forms of CL-instability are recognised:

1. **CL1-type** in which the vorticity-component ω_x can be generated by a Stokes drift which varies in the lateral direction

2. **CL2-type** in which the vorticity component ω_x may be generated by a lateral uniform Stokes drift acting on a pre-existing vertical vorticity ω_z.

The CL2-type instability is described by Leibovich (1977) and amounts to the following. It is supposed that the wind stress has produced a parallel shear flow $\overline{u}(z)$ and a Stokes drift $\overline{u}^S(z)$. A perturbation of the shear flow is now considered such that the total flow is described by $(\overline{u}(z) + \hat{u}, \hat{v}, \hat{w})^T$. A perturbation of the pressure is not needed here. Then, the following behaviour of the perturbations is considered:

$$\hat{w} = \phi(z) \exp\left[\sigma t + i\,(my + kz)\right] \quad , \quad \hat{u} = \frac{1}{(m^2 + k^2)} \left(ik\hat{w}_z - m^2 \hat{w} \frac{\tilde{u}}{f}\right)$$

$$\hat{v} = \frac{m}{(m^2 + k^2)} \left(i\hat{w}_z + k\hat{w}\frac{\tilde{u}}{f}\right) \quad , \quad f = \sigma + ik\left(\overline{u} + \overline{u}^S\right)\,,$$

with $\tilde{u}$ being the wave part of the current. For $\phi(z)$ then is obtained in the non-viscous approximation the Rayleigh equation

$$\frac{\partial^2\phi}{\partial z^2} - \left(m^2 + k^2\right)\phi + \left\{\frac{k}{if}\frac{\partial^2\overline{u}}{\partial z^2} + \frac{m^2}{f^2}\frac{\partial\overline{u}}{\partial z}\frac{\partial\overline{u}^S}{\partial z}\right\}\phi = 0\,. \tag{9}$$

With the further simplification of rolls aligned with the mean flow (i.e., $k = 0$) we get

$$\sigma^2\left(\frac{\partial^2\phi}{\partial z^2} - m^2\phi\right) + m^2\mathcal{M}(z)\phi = 0 \quad \text{with} \quad \mathcal{M}(z) = \frac{\partial\overline{u}^S}{\partial z}\frac{\partial\overline{u}}{\partial z}\,. \tag{10}$$

The condition for instability now reads $\mathcal{M}(z) > 0$ anywhere in the interval for z. The corresponding maximum growth is $\mathcal{M}^{1/2}(0)$. For the growth of Langmuir circulations it is thus necessary that $\mathcal{M}(z)$ is positive anywhere in the fluid, in other words, a positive shear of the current is required because the Stokes drift diminishes for increasing depth. However, Nepf and Monismith (1991) found experimentally, in a flume, that vortices developped for both $\mathcal{M}(z) > 0$ and $\mathcal{M}(z) < 0$, see also the discussion in Nepf et al. (1995).

Manipulation of the vertical momentum equation

The numerical evaluation will be performed within an existing free-surface flow model in which the treatment of the vertical momentum equation will be worked out in a number of ways.

Hydrostatic approach

For the handling of the vertical momentum equation several possibilities exist. A very simple one consists of ignoring the vertical momentum equation altogether and determining the vertical velocity afterwards by an integration of the continuity equation in which the solutions u and v from the horizontal momentum equations are used. These horizontal momentum equations in most simple form are

$$\frac{du}{dt} + \frac{\partial\overline{\pi}}{\partial x} = \frac{1}{\rho}\frac{\partial\overline{\sigma}'_{k1}}{\partial x_k} \quad \text{and} \quad \frac{dv}{dt} + \frac{\partial\overline{\pi}}{\partial y} = \frac{1}{\rho}\frac{\partial\overline{\sigma}'_{k2}}{\partial x_k} + \overline{u}^S\frac{\partial u}{\partial y}\,. \tag{11}$$

One of the ways of explaining the measured mean current profiles is the following qualitative one. We consider waves and current in a laboratory flume. In the lateral (y) direction, changes in the velocity field should occur. This has to be generated by the wall effects. The basic idea is as follows. Suppose that a circulation cell has developped. Suppose that the cell is such that in the middle of the flume the flow is in downward direction. The situation is as sketched in Figure 2. In the upper part of the fluid, water with a small amount of momentum is transported towards the middle of the flume and consequently decelerates, while in the lower part of the fluid the reverse situation occurs. In the upper half of

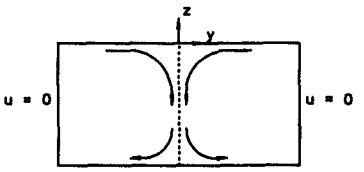

Figure 2: Flow in a lateral vertical section

the fluid the downward velocity increases and in the lower half it decreases. In the middle of the flume $\partial v/\partial y = 0$ because of symmetry. From the continuity equation $u_x + w_z = 0$ in the middle of the flume then follows that $\partial u/\partial x < 0$ in the upper half and $\partial u/\partial x > 0$ in the lower half of the fluid. Consequently, the profile $u(z)$ turns back in the upper part of the fluid and increases in the lower part. The result is a more uniform horizontal velocity profile in the vertical.

A semi-Poisson approach

A more precise formulation consists of splitting the pressure in a hydrostatic and a non-hydrostatic part. The solution procedure then consists of two steps. In the first step only the hydrostatic part of the pressure is used and in the second step a Poisson equation for the non-hydrostatic part has to be solved. Such a method has also been used by Casulli (1995). We write the pressure as the sum of a hydrostatic part p_h and a non-hydrostatic part q: $p = p_h + q$. The computation is split in two parts.

Step 1

Consider the continuity equation and for the momentum equations we only use the hydrostatic part of the pressure. These momentum equations, which are to be solved in the first step then are, in vectorial form

$$\frac{d\overline{\boldsymbol{u}}}{dt} + \frac{1}{\rho}\operatorname{grad} p_h = -\boldsymbol{g} + \frac{1}{\rho}\operatorname{div}\overline{\boldsymbol{\sigma}}' \quad \text{with} \quad \boldsymbol{g} = (0,0,-g)^T \ . \tag{12}$$

Step 2

In the second step we consider the momentum equations without the convective terms and we only account for the non-hydrostatic part of the pressure. Furthermore the vortex force is accounted for here. We then have the system:

$$\frac{\partial\overline{\boldsymbol{u}}}{\partial t} + \frac{1}{\rho}\operatorname{grad} q = \overline{\boldsymbol{T}}_0 \tag{13}$$

with the vortex force $\overline{\boldsymbol{T}}_0$ given by (3).

We now apply the operation div on (13). For the velocities it is mandatory that $\operatorname{div}\overline{\boldsymbol{u}} = 0$ (i.e., the continuity equation is applied as a side condition because it was already used in the first step). The result is a Poisson equation for the

non-hydrostatic part of the pressure:

$$\mathrm{div}\left(\frac{1}{\rho}\,\mathrm{grad}\,q\right) = \mathrm{div}\left[\left(0, \overline{u}^S\frac{\partial u}{\partial y}, \overline{u}^S\frac{\partial u}{\partial z}\right)^T\right] \tag{14}$$

After solving the pressure part q of this Poisson equation, the solution q is substituted in Eq. (13) yielding new estimates for the velocities. This completes step 2.

Notice that the splitting is such that in step 1 a usual free-surface flow computation is performed. The second step gives the correction to the hydrostatic pressure, which correction is due to the vortex force. The vortex force, figuring at the right-hand side of the Poisson equation, is computed with the velocities estimated in the first step.

Numerical experiments

We now perform some computations to compare with the results of measurements of Klopman's physical experiments in the so-called Scheldt flume, which has a width of 1 m while the mean water depth in the experiments is 0.5 m. The walls of the flume are made of glass and are therefore hydraulically smooth. The bed was roughened with sand with a grain size of approximately 2 mm. The roughness of the bed was determined experimentally and the Nikuradse roughness was found to be 1 mm. The experimental set-up consists of two wave boards near each end of the flume; both wave boards generated waves and, at the same time, absorbed reflected waves. A discharge was generated with a constant outflow of 80 litres/s. For further details about the lay-out of these experiments we refer to Klopman (1994).

We only consider the regular-wave experiments. The main parameters are

wave period	$T = 1.44\,\mathrm{s}$
wave amplitude	$a = 0.06\,\mathrm{m}$
current velocity	$\overline{u} = 0.16\,\mathrm{m/s}$
mean depth	$h = 0.50\,\mathrm{m}$
bottom roughness height	$z_0 = 0.04\,\mathrm{mm}$

Following waves

In order to obtain enough shear for the CL-vortex force to be effective, the computations are started first without the CL force included and as initial value a uniform velocity of 0.16 m/s is used, whereas the turbulent kinetic energy $\mathbf{k}$ and the dissipation ϵ are initially taken to be zero. After 200 s the turbulent logarithmic shear flow has developped sufficiently for the CL-vortex force to be effective. From that moment on the CL-vortex force is included in the computations. At t = 300 s a new steady state is obtained with two eddies in the cross-section of

the flume. For the situation of waves following the current, the velocity profile in a cross section of the flume has been shown in Fig. 3. The development of the

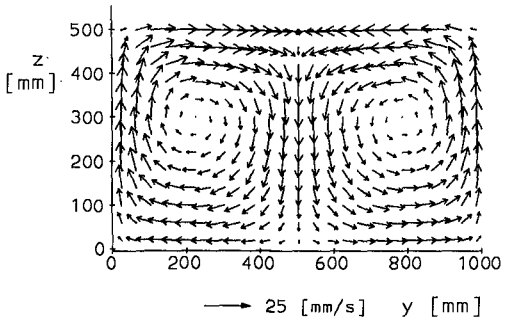

Figure 3: Velocity field in cross section at time $t = 300$ s.

vertical profile of the horizontal velocity in time is shown at the left-hand side of Fig. 4; the time that logarithmic profile is developped is now taken as the origin of the time-axis for the further discussion.

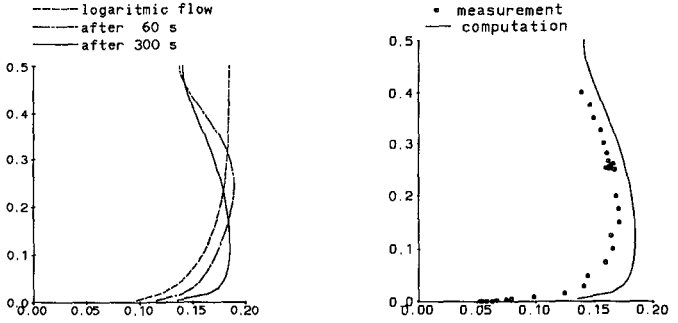

Figure 4: Development in time of the vertical profile of the horizontal velocity for the situation of waves following the current *(left)*; Comparison of the vertical profile for following waves with the measured profile *(right)*.

Because in the measurements a reference velocity, averaged over the depth, was based on the total flow, with the assumption of uniform flow over the width of the flume, a correction procedure is necessary now to account for the side-wall effects. For the situation of current alone (no waves) the computed vertically averaged horizontal velocity, evaluated in the centre of the flume, was taken as reference for the vertically averaged velocity as resulting from the measurements, likewise taken in the centre of the flume. This requires an enlargement of the measured velocity in the centre of the flume by a factor 1.135. This factor has been applied to all measurements, also those with following and opposing waves. The comparison of the vertical profile of the computation and the measurement with this correction is shown at the right-hand side of Fig. 4. The inclusion

of the CL-vortex force thus has, for following waves, the effect of increasing the near-bottom horizontal velocity and decreasing the horizontal velocity near the free surface, as was also measured. The profile of the current over the width of the flume is shown for a height of 5 cm above the bottom at the left-hand side of Fig. 5. At the right-hand side is shown the development of the vertical current in the centre of the flume.

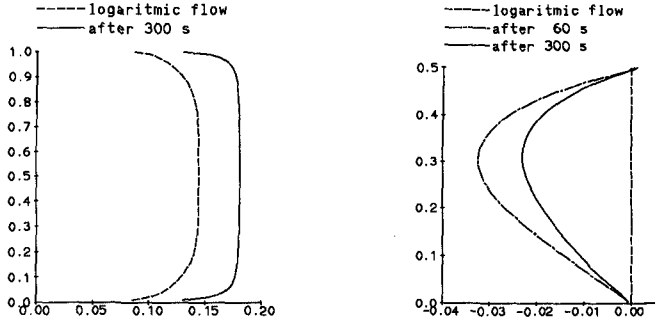

Figure 5: The horizontal current across the width of the flume for following waves, without waves (the logarithmic profile) and 300 s later (with waves); development in time of the vertical profile of the vertical velocity for the situation of waves following the current *(right)*; Comparison of the vertical profile for following waves withe the measured profile *(right)*.

A test on the possibility of Langmuir circulations was devised by taking a very wide flume with otherwise the same parameters. In this situation also only two circulation cells developped and therefore the possibility of obtaining true Langmuir circulations is ruled out for this situation. In the present situation the flow is boundary-driven. The rigid side walls act as an agent for the development of the circulation cells.

Waves propagating against the current

Also in this case two eddies are generated, rotating in opposite directions as those generated for waves propagating in the same direction as the current. This is as was expected. The development of the vertical profile for the horizontal current is shown in Fig. 6. This shows that the flow near the bed is reduced, and that the flow near the free surface is not increased as was to be expected. Notice that Nepf and Monismith (1991) found from measurements in a flume for both waves following and against the current that circulation cells developped. This is also the case in the present computations. Why almost no effect on the current profile is found for opposing waves is not yet clear. This deserves further investigation.

Conclusion

The numerical experiments lead to the following conclusions.

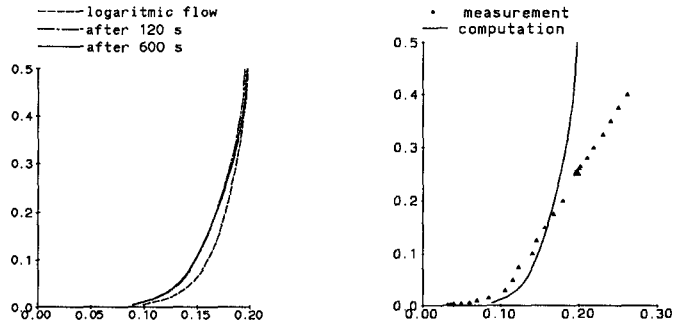

Figure 6: Development in time of the vertical profile of the horizontal velocity for the situation of waves propagating against the current *(left)*; Comparison of the vertical profile of the horizontal velocity for waves propagating against the current with the measured profile *(right)*.

1. Because also for a very wide flume only two circulation cells will develop, we conclude that the possibility of Langmuir circulation is ruled out for this situation. The flow is boundary-driven.

2. The principal mechanism of change of the near-surface velocities is the lateral transport of low-momentum fluid from the rigid side walls to the centre of the flume. Therefore, we conclude that the CL-vortex force is, at least partly, responsible for the observed change in velocities due to waves upon currents.

3. For both following and opposing waves circulation cells are found in the computations, which is in accord with the experiments of Nepf et al. (1995). Why the case for opposing waves has so little effect on the change of the current profile compared to the case without waves is not yet clear and deserves further investigation.

Acknowledgement

This work was commissioned by the National Institute for Coastal and Marine Management/RIKZ of the Dutch Public Works Department.

References

[1] **Andrews, D.G. and McIntyre, M.E. (1978)**. An exact theory of nonlinear waves on a Lagrangian-mean flow. *J. Fluid Mech.* **89(4)**, pp. 609-646.

[2] **Bakhmetev, B.A., 1932**. *Hydraulics of Open Channels*, Eng. Soc. Monograph, McGraw-Hill.

[3] **Casulli, V., 1995**. Recent developments in semi-implicit numerical methods for free surface hydrodynamics. In: *Advances in Hydroscience and Engineering*, Vol. II, March 1995, Beijing, China, 8 pp.

[4] **Craik, A.D.D. and Leibovich, S., 1976**. A rational model for Langmuir circulations. *J. Fluid Mech.* **73(3)**, pp. 401-426.

[5] **Craik, A.D.D., 1982**. The generalized Lagrangian-mean equation and hydronamic stability. *J. Fluid Mech.* **125**, pp. 27-35.

[6] **Kemp, P.H. and Simons, R.R., 1982**. The interaction between waves and a turbulent current: waves propagating with the current. *J. Fluid Mech.* **116**, pp. 227-250.

[7] **Kemp, P.H. and Simons, R.R., 1983**. The interaction between waves and a turbulent current: waves propagating against the current. *J. Fluid Mech.* **130**, pp. 73-89.

[8] **Klopman, G. (1994)**. Vertical Structure of the flow due to waves and currents; Laser-Doppler flow measurements for waves following or opposing a current. *Delft Hydraulics*, Report **H840.30, Part II**.

[9] **Leibovich, S., 1977**. Convective instability of stably stratified water in the ocean. *J. Fluid Mech.* **82(3)**, pp. 561-581.

[10] **Leibovich, S., 1980**. On wave-current interaction theories of Langmuir circulations. *J. Fluid Mech.* **99(4)**, pp. 715-724.

[11] **Leibovich, S., 1983**. The form and dynamics of Langmuir circulations. *Annual Review of Fluid Mechanics* **15**, pp. 391-427.

[12] **Nepf, H.M. and Monismith, S.G., 1991**. Experimental study of wave-induced longitudinal vortices. *J. of Hydraulic Engineering* **117(12)**, pp. 1639-1649.

[13] **Nepf, H.M., Cowen, E.A., Kimmel, S.J. and Monismith, S.G., 1991**. Longitudianl vortices beneath breaking waves. *J. Geophys. Res.* **100(C8)**, pp. 16211-16221.